HANOI UNIVERSITY OF EDUCATION
FACULTY OF PHYSICS

DOAN THI THE

OPTICAL PROPERTIES OF A CHERENKOV COUNTER

DIPLOMA IN ASTROPHYSICS
SPECIALITY: ASTROPARTICLE PHYSICS

Supervisors: PROF. PIERRE DARRIULAT
MSc. PHAM NGOC DIEP

HANOI, MAY - 2007

INTRODUCTION

The present work was made at VATLY, the cosmic ray laboratory in Hanoi, which is associated with the Pierre Auger Observatory (PAO) in Argentina. The aim of the PAO is to study the very high energy end of the cosmic ray energy distribution where many questions are still unanswered. The first chapter is an introduction to cosmic ray physics and a brief presentation of the PAO. It is a hybrid detector including a fluorescence detector of the fly eye type and a surface detector made of an array of 1600 water Cherenkov counters. A replica of such a counter has been assembled and is being operated on the roof of VATLY. The second chapter describes a detailed study of the optical properties of such a counter. These govern the time structure of the signals recorded in the three light detectors that equip each Cherenkov tank. A detailed understanding of its properties is essential to exploit efficiently the PAO data. A Monte Carlo simulation based on a simple model has been used to perform this study. A major and particularly interesting result is the identification of a strong asymmetry between the three light detectors in the early part of their signals. This is the specific subject of Chapter 3 where the properties of this asymmetry are described and explained in some detail, together with its implication on the analysis of real data. The work is briefly summarized in a last section.

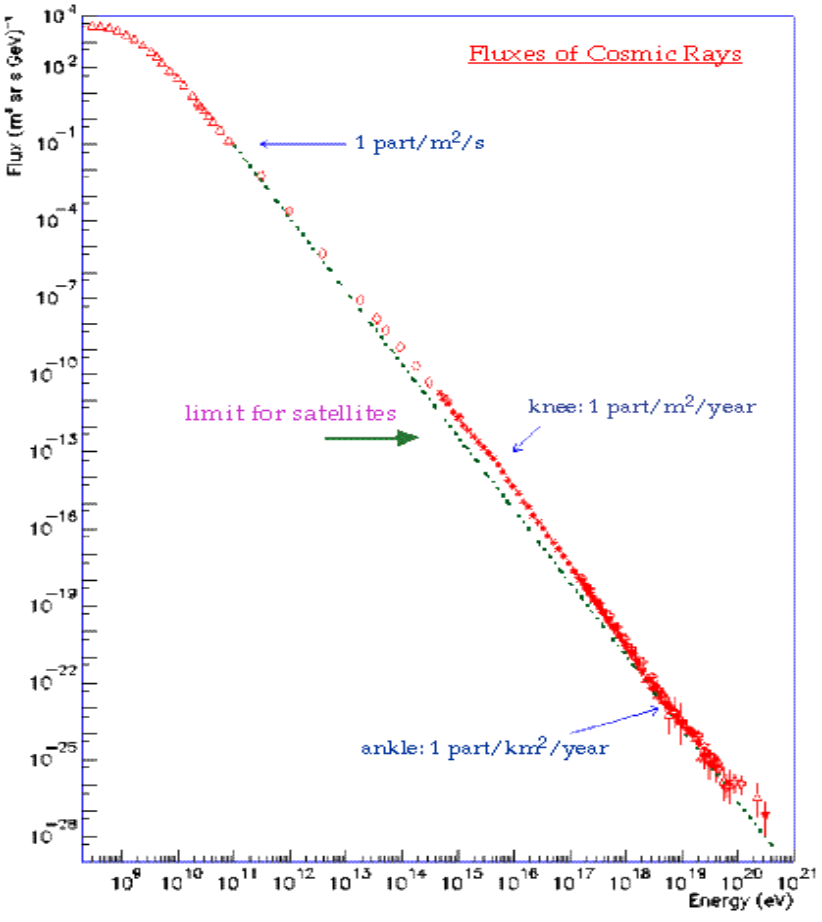

Figure 1. Cosmic ray primary energy spectrum

CHAPTER 1

COSMIC RAYS AND THE PIERRE AUGER OBSERVATORY (PAO)

1.1 Cosmic rays: general properties, energy spectrum and composition

Primary cosmic rays are charged particles (here, we do not include photons and neutrinos under this name) that travel in space with energies reaching of the order of 10^{11} GeV. The vast majority (~98 %) of these particles are ionized nuclei, mostly protons, with the remaining portion being primarily electrons [1]. Of the nuclei, 90% are measured to be protons, 9% are alpha particles and the remaining 1% heavier nuclei [2]. However, these abundance ratios are strongly energy dependent. The dependence of the differential flux of primary cosmic ray particles on energy is illustrated in Figure 1. It covers 32 orders of magnitude and is seen to obey an approximate power law [3] with an index that varies between 2.5 and 3.3. Modulations have been found in the form of changes of slope. While they are not understood in detail, they are related to thresholds associated with new sources becoming accessible. Indeed the magnetic fields existing at various scales, Earth, Solar system, Milky Way, shield the Earth from cosmic rays, introducing effective low energy cut offs in their spectrum. In Ha Noi, the so called "rigidity" cut-off caused by the Earth magnetic field amounts to 17 GeV. The change of slope referred to as the "knee", just above 10^6 GeV, is associated with the shielding effect of the galactic magnetic field [4]. Above this energy, cosmic rays are mostly of extragalactic origin and are isotropic (galactic cosmic rays being enhanced on the equator of the Milky Way). The so-called "ankle", just above 10^9 GeV, is not well understood. Above 10^{11} GeV, the spectrum is cut off by the so called GZK effect [5, 6] associated with the photoproduction of pions (either free or in the form of nucleon resonances) on the photons of the cosmic microwave background.

1.2 Origin and acceleration mechanism

While the existence of cosmic rays resulting from the decay of very massive primordial particles cannot be fully excluded, it is generally considered that cosmic rays are the result of an acceleration mechanism acting on charged particles in space. One may distinguish between three different scales, solar, galactic and extragalactic.

At least part of the very low energy cosmic rays originate in the outer layers of the Sun, from what is called the solar wind. Some active regions of the Sun

continuously emit particles with energies in the MeV range into interplanetary space and solar flares can sporadically accelerate particles up to several GeV/nucleon [7]. Above 0.1 GeV/nucleon, their contribution rapidly decreases. All stars are expected to emit stellar winds, in some cases significantly more energetic and with higher fluxes than the Sun. Their contribution to the cosmic ray spectrum extends to the TeV range or so.

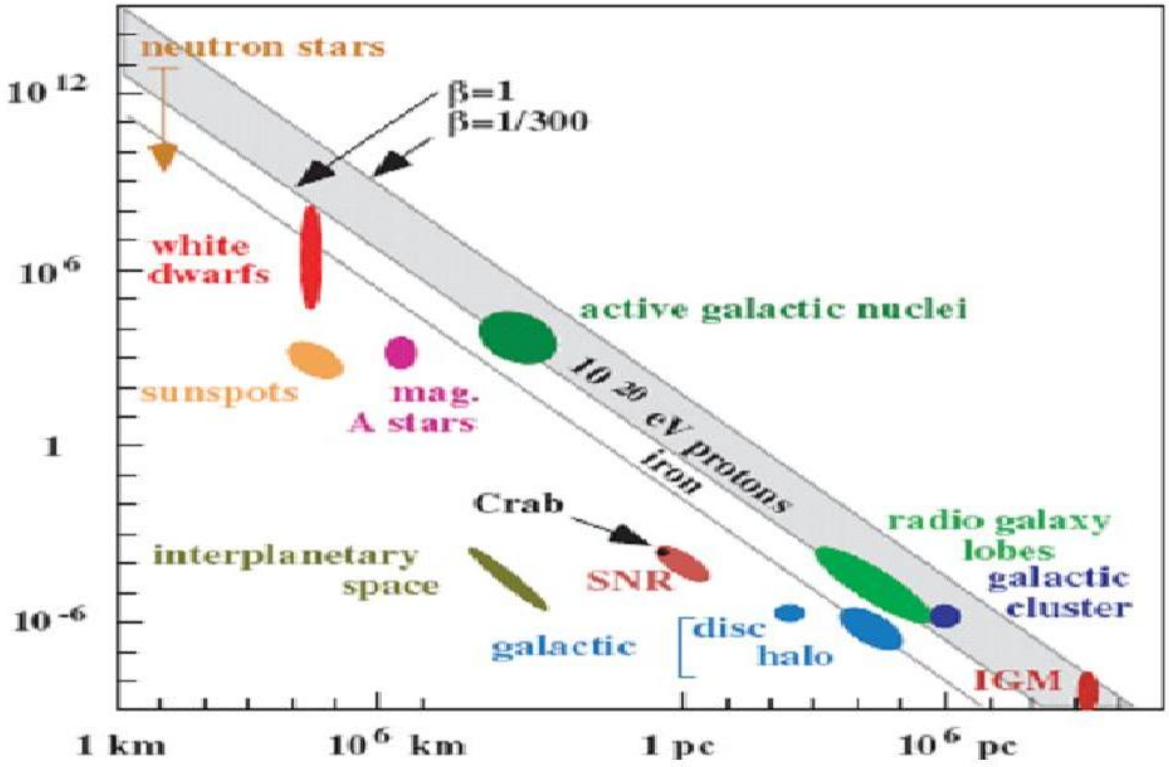

Figure 2. Hillas Plot showing the minimal value of the product BL (magnetic field × size) for accelerating a proton to 10^{20} eV. The limit is shown as a line in the logB(Gauss)−logL plot. A few candidate sites are indicated.

In the 10^3 TeV range, cosmic rays are known to originate mostly from supernova remnants (SNR), as evidenced by the study of very high energy cosmic gamma rays in detectors such as HESS [8]. Such high energy photons are understood as being decay products of neutral pions produced by the interaction of very high energy cosmic rays with the interstellar matter present in the surroundings of their sources. The acceleration mechanism invoked to explain these very high energy cosmic rays is called “diffusive shock acceleration”. It is induced by multitraversals of

the front of the shock wave produced at the time of the supernova explosion, by charged particles moving in a random walk in the magnetic fields present in the SNR environment. At yet higher energies, up to the GZK cut-off, it is usually believed that a similar mechanism is at play. The very high energies that may be reached place, however, very stringent constraints on possible sources that must be both very extended (compared to the magnetic bending radius) and the seat of strong magnetic fields (but in this context, "strong" may mean a few μG!). More concretely, it is the product of these two quantities that matters and the plot shown in Figure 2, the so-called Hillas plot, illustrates this fact in the case of 10^{11} GeV protons. First indications by Auger in favour of nearby AGN's being the sources of ultra high energy cosmic rays have been recently presented [9, 10].

1.3 Air showers

When a cosmic ray enters the Earth atmosphere, it generates a hadronic shower (Figure 3). It develops at a scale defined by the nuclear interaction length of protons in air (90 g/cm^2). The atmospheric density decreases with altitude, approximately as an exponential having a decay length of 7.8 km. At very high energies, the multiplicity at each interaction is high as are the energies of the secondaries: the cascade develops very deep in the atmosphere. At the PAO, a 10^{11} GeV vertical shower is barely reaching its maximum when hitting ground, with several billions particles covering a few square kilometres. The difference between a proton induced shower and a shower induced by a heavier nucleus is mostly a faster early development in the second case as the nucleons in the nucleus can be thought of as interacting independently with air nuclei. At each interaction mesons are produced, mostly pions, kaons and their resonances, while the incident nucleon continues its way as a "leading" nucleon retaining a large fraction of its energy (one talks of the inelasticity of the interaction as a measure of the difference between this fraction and unity). The mesons and meson resonances produced can be thought as promptly decaying into pions, either neutral or charged. While the neutral pions immediately decay into two photons, and are therefore lost for continuing the hadronic shower development (they contribute instead to the development of an electromagnetic shower containing electrons, positrons and photons), the charged pions are not: they will often live long enough to interact with the air nuclei. The relevant factor

measuring the competition between the two processes, interaction and decay, is the ratio between interaction and decay lengths (the latter multiplied by the very high gamma factor of the Lorentz boost). Charged pions decay into muons and neutrinos with a proper lifetime of 0.026 μs according to

$$\pi^{\pm} \rightarrow \mu^{\pm} + \nu_{\mu} \,(\text{anti}\nu_{\mu}).$$

Muons decay in turn into electrons and neutrinos, however with a much larger lifetime (2.2 μs).

When reaching ground, a very high energy shower is therefore dominated by its photon and electron component, the photons of the neutral pion decays having generated electromagnetic showers with a scale defined by the radiation length in air, 37 g/cm^2. The muon fraction is, however, strong enough to be detected and is observed to be a good discriminator between proton induced showers and showers induced by heavier nuclei.

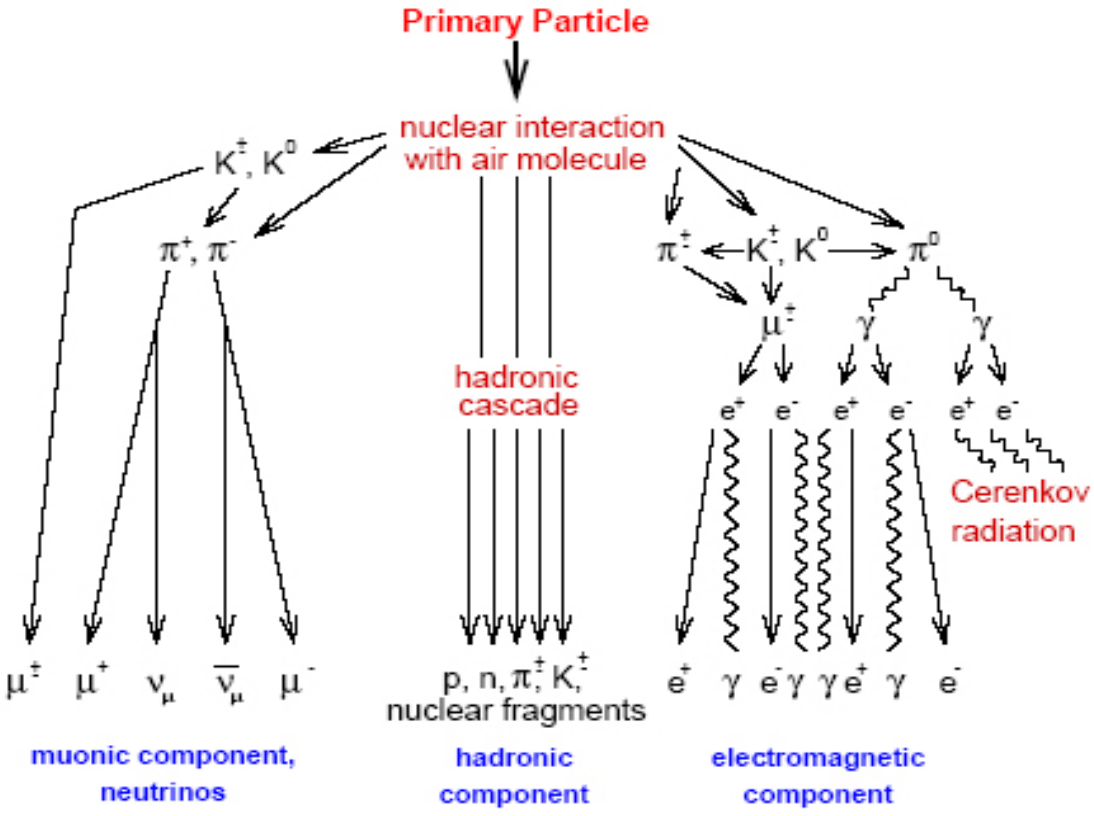

Figure 3. Schematic representation of the shower development

1.4 The PAO, a hybrid detector

Very high energy cosmic rays are detected from the extensive air showers which they produce in the atmosphere. There exist two main methods of detection, one consisting in sampling the particle density on ground and the other in detecting the fluorescence light produced on nitrogen molecules along the shower [11]. These methods have been used, or are being used, by several experiments such as Volcano Ranch, Haverah Park and AGASA for the surface detector arrays, and Fly's Eye and HiRes for fluorescence detectors. In both cases an accurate measurement of the arrival time of the measured signals makes it possible to measure the direction in the sky from which the primary cosmic ray is reaching us. But the two methods are otherwise very different: fluorescence detectors measure the longitudinal profile of the shower development, the integral of which is a direct measure of the energy [12]. Surface detectors measure instead the transverse profile of the shower at that particular stage of its development that it happens to be in when reaching ground. Its lateral extension also provides a measure of the shower energy, however much less direct than in the fluorescence case. But the fluorescence measurement is significantly more difficult than sampling on ground and its duty cycle is only 10% as it can only be made during moonless clear nights. As a result, all in all, both methods are of comparable value. Yet, as the systematic uncertainties contributing to them are so different, the value of being able to use both of them simultaneously as is the case in the PAO is an invaluable asset.

The PAO was therefore designed as a hybrid detector with the ability to reach the highest energies, 10^{11} GeV, with a good statistical significance. It is under current completion in the Argentina pampas and can explore the whole austral sky, including the centre of the Milky Way.

1.5 Transverse shower profile, surface detector

Both plastic scintillators and water Cherenkov counters have been used efficiently in the ground detection of showers. They behave differently. Scintillators respond to all charged particles in proportion to their energy loss in the medium while Cherenkov counters respond to charged particles having a β in excess of $1/n$, n being the refraction index of the radiator, 4/3 in the case of water. The number of photons produced by a minimum ionizing particle is of the order 20000 photons/cm in

comparison with some 200 photons/cm in a water Cherenkov counter [13]. A major difference between scintillators and Cherenkov counters is the ability of the latter to convert nearly all photons, as the radiation length is of the order of 40 cm in both materials: a typical scintillator radiator is a few percent of a radiation length thick while a typical Cherenkov radiator is several radiation lengths thick. Indeed, as scintillators are expensive, they are usually made in the form of relatively thin plates (a few centimetres) that offer a cross-section to the shower that is proportional to the cosine of the zenith angle. The water Cherenkov detectors are much cheaper and can have instead a shape having similar dimensions in height and lateral extension, thereby offering to the shower a cross-section that is nearly independent of zenith angle. In practice a water depth of one meter or so is easy to implement and gives as much light as a one centimetre thick scintillator plate in the case of a minimum ionizing particle. Cherenkov counters, which were finally selected for the Auger surface detector for their lower price and good performance, are therefore very efficient detectors of soft electromagnetic showers which make up a large fraction of their signal.

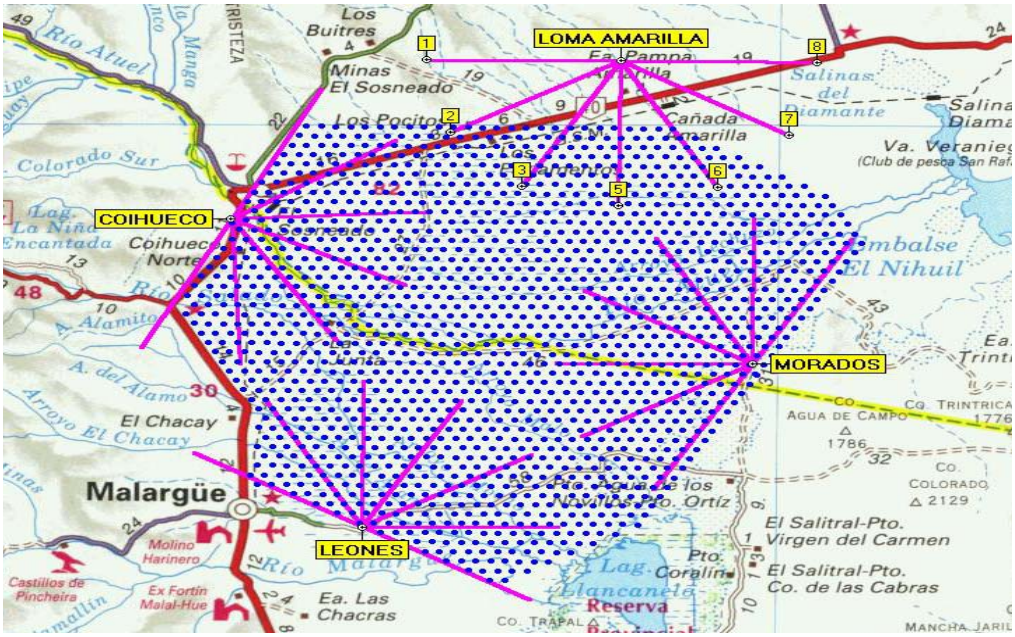

Figure 4. Map of the PAO site. Each dot represents the position of a Cherenkov tank. The array is viewed from four sides by fluorescent four sides by fluorescent.

The PAO surface detector (Figure 4) includes 1600 water Cherenkov tanks covering an area of 3000 km^2 [14]. They are located at the vertices of a triangular lattice having a mesh size of 1.5 km (closest distance between two counters). Each tank (Figure 5) contains a volume of 1.2 m×10 m^2 of high purity water. The Cherenkov light produced by fast shower particles crossing the water is detected by three 9'' photomultipliers. Their signals are recorded, in 25 ns bins, in flash analog to digital converters (FADC's) equipping both the anode and last dynode. A reasonably low threshold is used, well below the signal given by relativistic minimum ionizing particles.

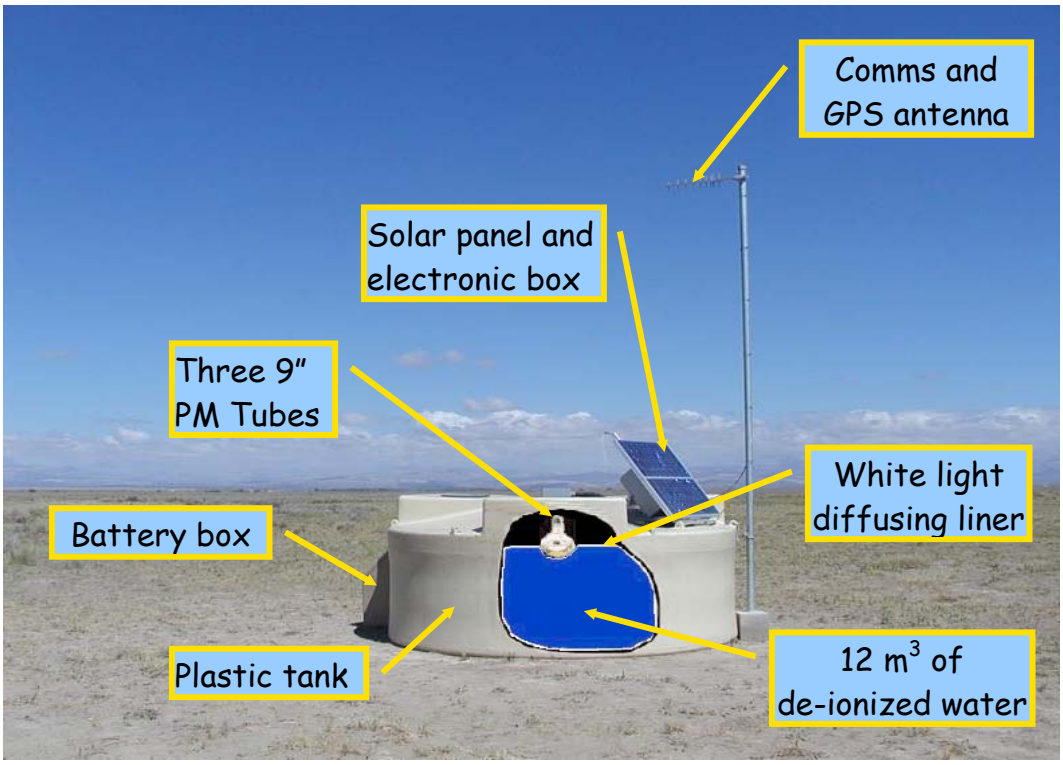

Figure 5. Exploded view of an Auger Cherenkov tank.

CHAPTER 2

THE RESPONSE OF THE PAO CHERENKOV COUNTERS

2.1 Motivation

In the Pierre Auger Observatory (PAO), charged particles are detected in water Cherenkov counters. A replica of such a counter has been assembled and studied at VATLY (Vietnam Auger Training Laboratory), the cosmic ray laboratory in Ha Noi. The study of its response to muons has shown that the signal produced is essentially proportional [15] to the length of the muon trajectory in the water volume (hereafter called track length). The muon trajectory depends on four parameters: the two coordinates of the impact point on ground, the zenith angle and the azimuth. Data available from the PAO make it possible to reconstruct the zenith angle and azimuth with a good accuracy (at most a few degrees). This measurement relies on a comparison between the times of arrival of the signal in the different tanks hit by the shower. As the shower front can be considered as being planar and isochronous (all shower secondaries travel at speed of light) it is sufficient to have three tanks hit to reconstruct the three parameters defining the shower direction (two angles) and mean time of arrival (one parameter).

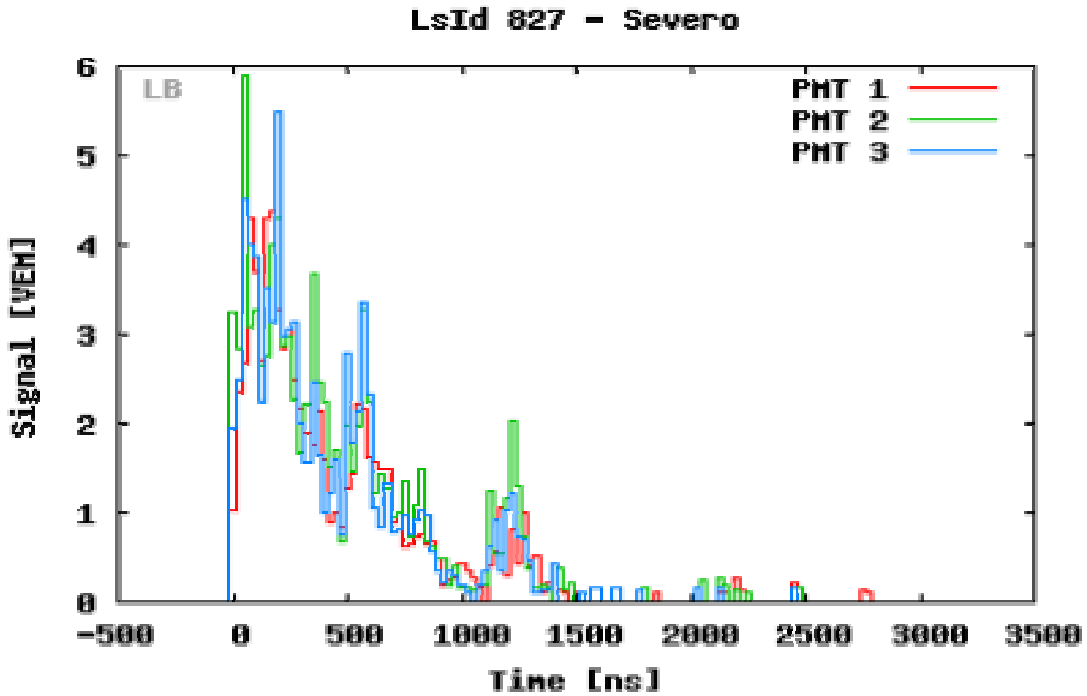

Figure 6. A typical FADC trace.

Each of the three PMTs of a Cherenkov counter records the time sequences of the signal it receives in its FADC, these are called FADC traces. A typical trace is shown in Figure 6. Each trace is made of a sequence of signals, possibly overlapping, each signal being generated by a shower particle hitting the Cherenkov tank. Disentangling the various signals that make up a trace is a difficult task. However, it is important to do it as accurately as possible in order to sort out the electron-photon component from the muon component in the shower products. Such an information is of great interest, in particular for the identification of the nature of the primary, proton or heavier nucleus. Muons can be identified on a statistical basis [16] if one knows which signal they are expected to give on average. However, on an event by event basis, since the muon impact point is unknown, so are the track length and the expected signal. All what is known is the expected track length distribution, which depends on zenith angle exclusively (the azimuth information is irrelevant in this respect). However, when considering the three PMT FADC traces individually, a dependence on azimuth of the PMT signals relative to each other, or relative to their mean, can be expected. It is therefore useful to know, in the case of a muon incident at angle of θ, not only what is the expected track length distribution, but also which are the expected FADC signals as a function of incidence angle θ and of the azimuth φ. The present note addresses these problems, using a Monte Carlo simulation of the production of Cherenkov light in the tank, of its propagation in water and of its diffusion from the walls.

2.2 Monte Carlo method

An analytic calculation of the main quantities that define the behaviour of the counter is in general impossible, or at least impractical. Too many parameters need to be averaged upon. For example, if one wishes to calculate the distribution of the number of photons produced by a vertical muon having its impact on the middle of the top plate, one has to integrate over the angle of each photon around the muon track, over its source point on the muon track, over its diffusions on the walls until it reaches one of the three phototubes, etc. Each of these integrations implies a convolution with the probability distribution of the quantity on which one integrates. The result is a single distribution and the calculation has to be repeated for each incidence angle and impact point of the muon. Moreover, if one wishes to calculate another distribution, for example that of the number of diffusions on the walls, a

completely new calculation has to be done. It is simply out of question. What one does in practice is to use a method which solves all these problems at once: the idea is to build up (in a computer) a sample of a large number of "events" that simulate the true events, in that case the production of Cherenkov photons and their optical journey to the tank PMTs. If one has generated enough such events, and if each of them obeys the laws that govern real events, the distribution of any quantity on the generated event sample will be identical to that of real events. One says that one has simulated the real events, one talks of a "simulation" of the problem. The advantage is double: it avoids any complicated calculation and it makes it possible to look at any distribution one may dream of without having to repeat the calculation. Technically, the limitation of the method is only statistical: one needs to generate large enough an event sample for the fluctuations to be negligible. In the present work we used samples of 10 000 generated events, which corresponds to 1% uncertainties ($1/\sqrt{10000}$). Practically, however, the real limitation of the method is that the simulation can not produce more than it was given as input, it has no intelligence, it simply has to be as faithful as possible to the truth. If some effect of relevance to the problem is ignored, or wrongly simulated, the result will be wrong of course. This method of calculation is widely used in modern physics and is named Monte Carlo after the name of a place in the south of France which is famous for its gambling casino (a random number generator is an essential tool of the method, each time a quantity has to be chosen – instead of being integrated upon – it is chosen at random with its proper distribution). The method is also used for the design of new objects, new detectors in the present case: one can optimize the parameters of the design on simulated objects before constructing a real prototype.

2.3 Geometry and track length in water

The tank is a cylinder, 1.2 m high and its 1.8 m in radius. Here we choose a Cartesian coordinate system with origin O at the center of the tank, Oz vertical pointing upwards.

Because of the revolution symmetry of the problem, the track length is calculated for particle trajectories in zOx plane. The angle of incidence is θ, ζ is an axis perpendicular to the particle's trajectory (see Figure 7).

If $\vec{u}$ is a unit vector along the particle trajectory, its projections on the axes are:

$$\vec{u} = (u_x, u_y, u_z) = (\sin\theta, 0, \cos\theta) \qquad (1)$$

A (x_i, y_i, z_i) being the projection of the O on the particle trajectory, the coordinates of the intersections (entrance and exit) of the track with the tank read:

$$x = x_i + \lambda u_x \quad (2)$$

$$y = y_i + \lambda u_y \quad (3)$$

$$z = z_i + \lambda u_z \quad (4)$$

where λ is a parameter depending on the incident muon trajectory.

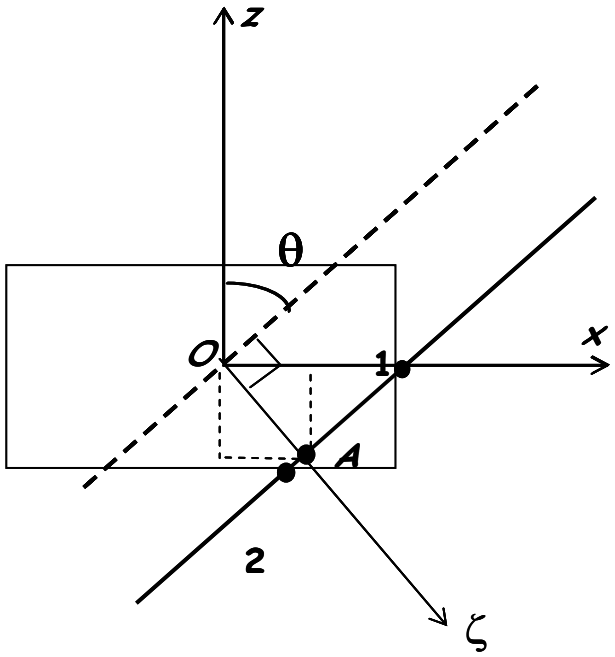

Figure 7. Definition of parameters used to describe particle trajectory entering a Cherenkov tank. The drawing is in the xOz plane. **A** is the projection of the tank centre on the track. **1** and **2** are intersections with the tank.

The track may intersect the tank on the top or bottom plates or on the side walls. The number of intersections can be *0* (when the particle misses the tank), or *2* (when the particle enters the tank).

Muon trajectories are generated with uniform *OA* and $\cos\theta$ distributions, that is isotropic. The azimuth distribution is also uniform and obtained by rotating the tank around its axis randomly between 0 and 360^o. However, as said earlier, for the track length calculation, this rotation can be omitted.

Intersection with the top plate:

Setting $z=0.6$ (all calculations are made in meters), from (4) we obtain $\lambda = (0.6-z_i)/u_z$; the x and y coordinates of the intersection with the plane of the top plate are calculated by inserting the value of λ in (2) and (3). If the condition $x^2+y^2 \leq 1.8^2$ is obeyed, this intersection is validated.

Intersection with the bottom plate:

The intersection is calculated as above, except for z being set to - 0.6.

Intersection with the side wall:

Replacing x and y from (2) and (3) into $x^2+y^2=1.8^2$ to solve for λ_1 and λ_2, we find the z coordinates of the two intersections: $z_1 = z_i + \lambda_1 u_z$ and $z_2 = z_i + \lambda_2 u_z$. If the relations $/z_1 /< 0.6$ or $/z_2 /< 0.6$ are obeyed, the corresponding intersections are validated.

2.4 Cherenkov light generation and propagation

Whenever the muon trajectory crosses the tank with a track length larger than 1mm, Cherenkov light is generated [13]. The number of Cherenkov photons per cm of water for a fully relativistic muon (which in practice is the case of virtually all muons) is expected to be $370 \sin^2\theta_C$ *per eVcm* where θ_C is the half aperture of the Cherenkov cone, namely $\cos\theta_C = 3/4$ and $\sin\theta_C = \sqrt{7}/4$, $\theta_C = 41.4^o$. Taking an accepted wavelength range in the visible between 0.4 and 0.7μm ($\Delta E = h\Delta\nu = hc\Delta\lambda/\lambda^2 = 2\pi\hbar c\Delta\lambda/\lambda^2 = 1$ *eV*) gives 162 photons per cm. Another estimate (with an effective photocathode sensitivity between 0.35 and 0.55 μm gives 208 photons per cm. In principle, one should account for the wave length dependence of the Cherenkov emission as well as of the photocathode efficiency and water transparency, but this is an unnecessary complication, it is sufficient to take an average value. In practice, assuming a photocathode efficiency of 20 to 25%, we generate 40 photons per cm step with full photocathode efficiency. Each photon is generated with a uniform azimuthal distribution around the muon track on a cone of half aperture θ_C. Each photon travels a length L and experiences a number n_d of diffusions before reaching one of the three phototubes. Each diffusion redirects the photon in the water, according to Lambert's cosine law. A diffusion probability of P_{diff}=95% and a water attenuation length of L_{att}=100m are used in the simulation: in practice, each photon reaching a photomultiplier tube is given a weight of $e^{-L/Latt}(0.95)^{nd}$. A photon is considered to be recorded in a PMT as soon as it reaches the top tank plate at a distance of less than

11.43cm from the centre of the PMT photocathode, that is on a circle of 1.2m centered on the tank axis. The three PMTs are symmetrically positioned at an azimuthal difference of 120^o with respect to each other. Photons hitting the corners between the cylindrical wall and the top or bottom plates to within less than a tenth of a millimeter are lost. So are also those which are diffused at grazing incidence to the walls, to within a tenth of a milliradian.

Photons reaching the photocathode of a PMT are recorded in its FADC trace, with an amplitude equal to the weight defined earlier and in a 25ns wide bin corresponding to the time of arrival of the photon on the photocathode. The origin of time is given by the instant at which the muon enters the tank (note that the muon travels at velocity *c* while the photons travel at velocity *3c/4*).

2.5 Track length distributions

When searching for muons in real data, it is useful to know which kind of charge distribution is expected for a muon at the particular angle of incidence of the shower. The impact point of the muon is unknown, but its angle of incidence is expected to be close to that of the shower. It is not exactly equal to it because the muon does not come from infinity: a small correction must be applied which accounts for this effect on average. Far from the shower core, the importance of the effect is significant. As the charge collected (averaged over the three PMTs) is to an excellent approximation proportional to the track length, it is useful to have a set of track length distributions calculated for different angles of incidence.

The track length is calculated using the relation:

$l = \sqrt{(x_2-x_1)^2 + (y_2-y_1)^2 + (z_2-z_1)^2}$

The resulting distributions are shown in Figure 8 above for ten different bins of $\cos\theta$.

For nearly horizontal incidences ($\cos\theta$ between 0 and 0.1, see Fig.8a) the track length varies between 0 and a maximum value of 3.6m, the latter being however more likely: For $\cos\theta=0$, the track length is $l=2\sqrt{(1.8^2-y^2)}$ and, as $dN/dy = cte$, $dN/dl \propto dy/dl \propto l/\sqrt{(1-[l/2R]^2)}$.

For nearly vertical incidence, $l=1.2m$ (Figure 8j).

In between a transition occurs when the incidence angle corresponds to the diagonal of the tank ($cos\theta=0.32$), for which the track length is $\sqrt{(3.6^2+1.2^2)}=3.8m$, the largest possible value for the track length (Fig.8d).

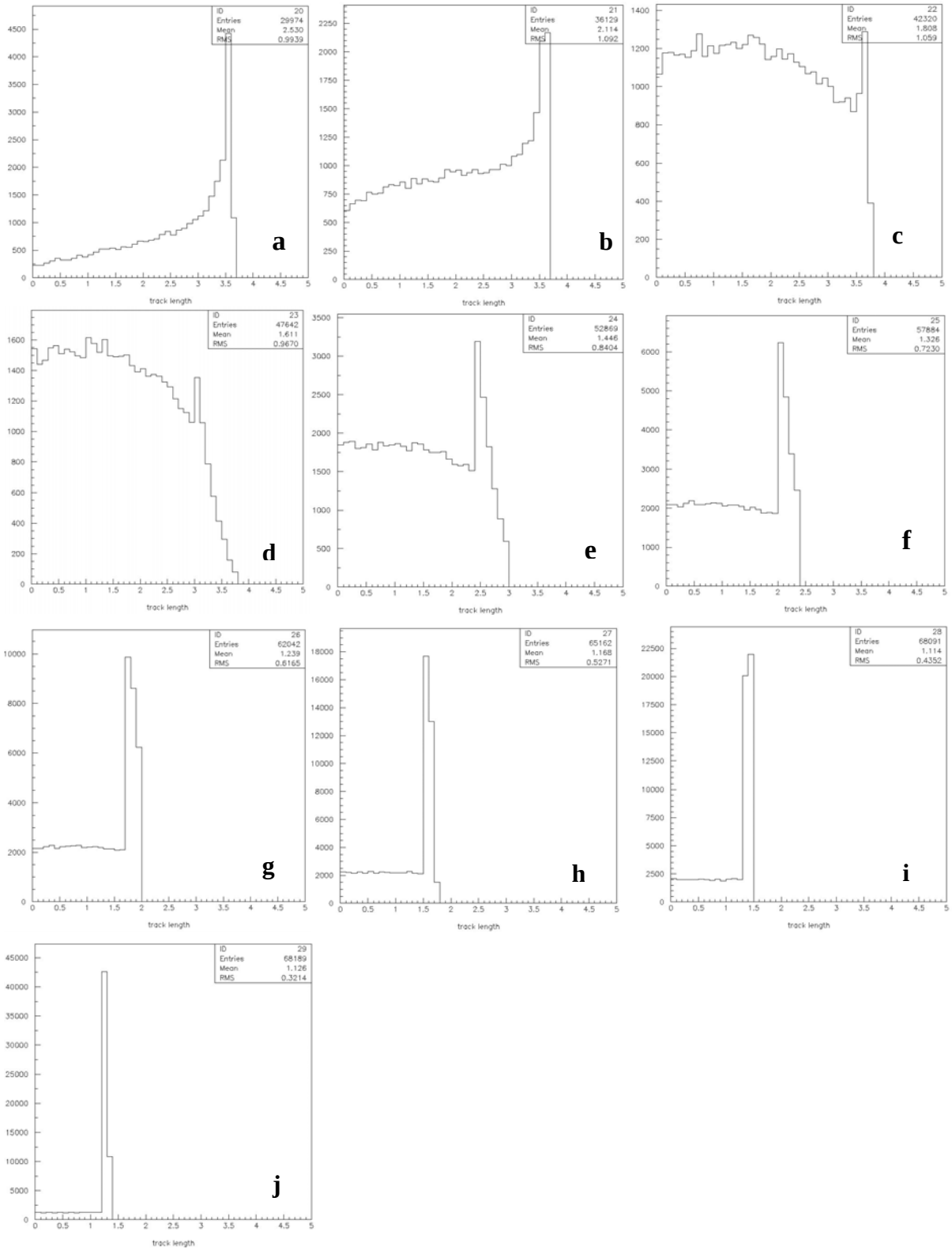

Figure 8. Track length distributions in different bins of $\cos\theta$. Each bin is 0.1 wide: 0 to 0.1, 0.1 to 0.2,…0.9 to 1.0 going from top left (panel a) to bottom right (panel j).

The table below lists the mean and rms values of the track length distributions obtained in each of the $cos\theta$ bin.

Table 1.

$<cos\theta>$	$<\theta>$	$< l >$	***Rms* (*l*)**
0.05	87.1	2.53	0.99
0.15	81.3	2.11	1.09
0.25	75.5	1.81	1.06
0.35	69.5	1.61	0.97
0.45	63.3	1.45	0.84
0.55	56.6	1.33	0.72
0.65	49.5	1.24	0.62
0.75	41.4	1.17	0.53
0.85	31.8	1.11	0.44
0.95	18.2	1.13	0.32

2.6 General properties of the FADC traces

In a first step we generate three sets of data corresponding to different incidences: one isotropic between 0^o and 90^o, one vertical and one at 80^o. For each of these we show a number of distributions in Figures 9 to 12.

Figure 9 shows the distribution of the number of diffusions experienced by each Cherenkov photon and Figure 10 shows that of the total length of its journey in water before reaching a PMT (or being lost). The average values of these two quantities are 14 and 20 respectively. Figure 11 shows the FADC trace, averaged over the three PMTs and all muons and Figure 12 shows the correlation of its integral with the track length.

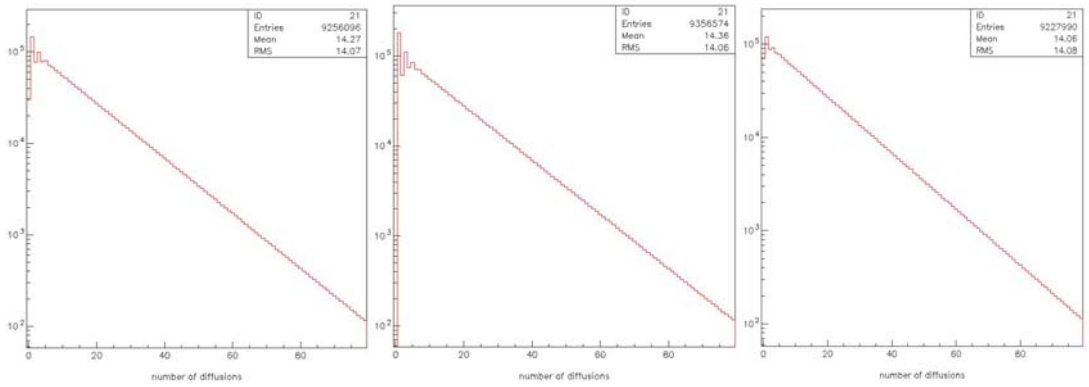

Figure 9. Distribution of the number of diffusions experienced by each Cherenkov photon (left, isotropic; middle, vertical; right, 80^{o})

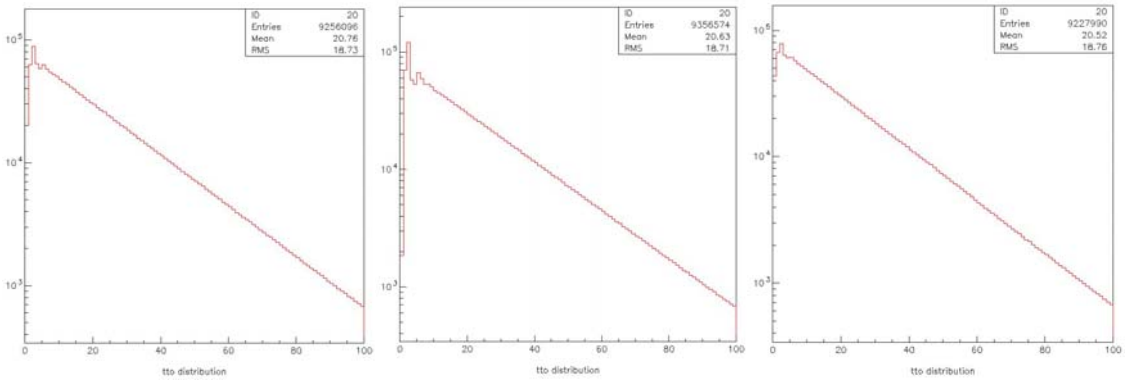

Figure 10. Distribution of the total length of the journey in water of each Cherenkov photon before reaching a PMT (or being lost) (left, isotropic; middle, vertical; right, 80^{o}).

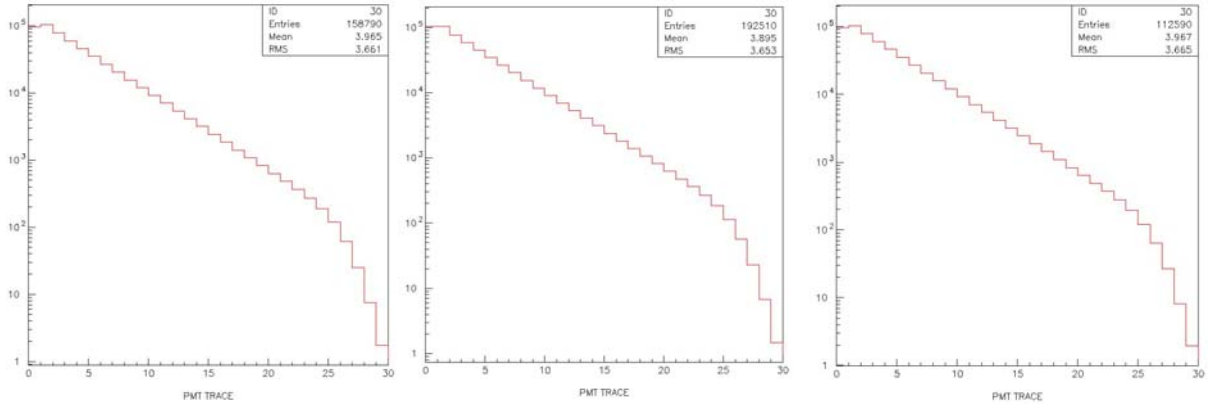

Figure 11. Mean FADC trace, averaged over the three PMTs and all muons (left, isotropic; middle, vertical; right, 80^{o}).

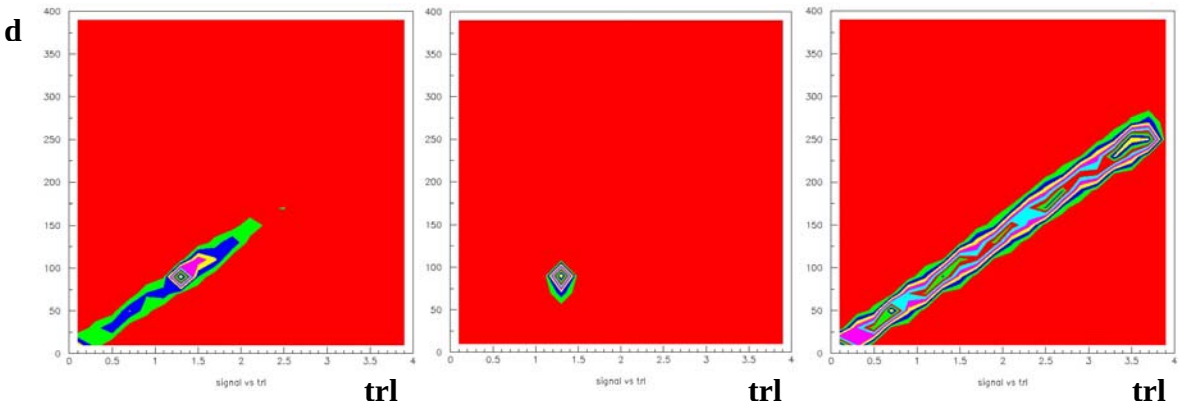

Figure 12. Correlation of the integral mean trace with track length (left, isotropic; middle, vertical; right, 80^{o}).

CHAPTER 3

ASYMMETRY OF EARLY PHOTONS

3.1 Evidence for the asymmetry

A remarkable feature of the simulation is the evidence it provides for a strong asymmetry between the three PMTs for the Cherenkov light that reaches them in the first nanoseconds. We define for each FADC bin a $\chi^2_{asym} = \sum (x_i - x_{mean})^2$ where the sum is over the three PMTs and x_i is the charge collected in that bin of PMT i , x_{mean} being the mean of the x_i. Figure 13 shows, for an isotropic muon distribution, the dependence of χ^2_{asym} over the FADC bins: it takes very large values in the first bin. Figure 14 shows the χ^2_{asym} distribution in each of the first five FADC bins separately. Two parameters are found to be relevant to the sharing of the early light among the three PMTs: the proximity of the muon track to the PMT photocathode and the azimuthal difference between the muon track and the PMT (with respect to the tank centre).

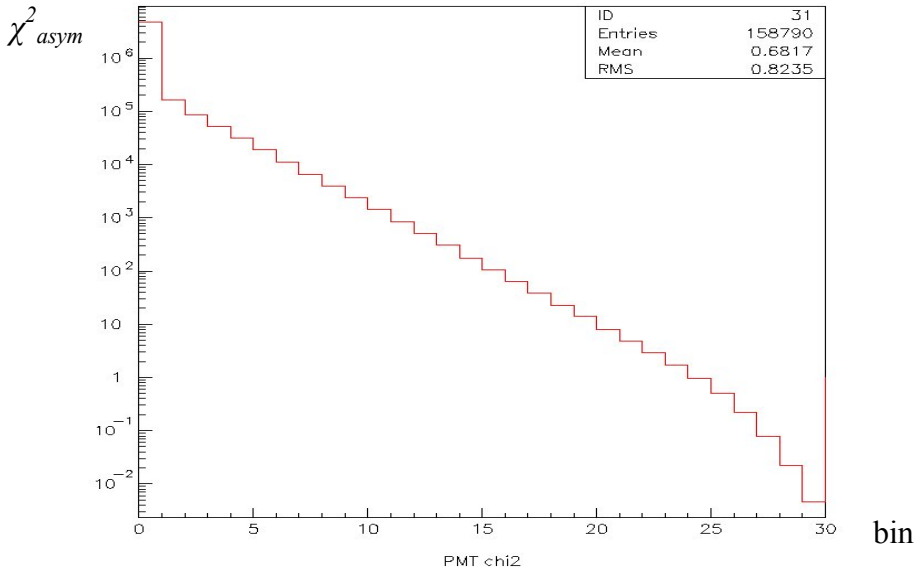

Figure 13. Distribution of χ^2_{asym} over the FADC bins (isotropic case).

Quantitatively, we define two quantities: d_i, the closest distance of approach of the muon track to the centre of the PMT i photocathode, and $\gamma_i = \boldsymbol{u}.\boldsymbol{v_i}$ the scalar product of the unit vector $\boldsymbol{u}$ on the muon trajectory, (the muons flies toward $-\boldsymbol{u}$) and the unit vector $\boldsymbol{v_i}$ joining the centre of the top tank plate to that of the PMTi photocathode. Distributions of d_i and γ_i are shown separately for the PMT having the

largest first bin charge, that having the second larger and that having the smallest in Figures 15 to 17. Figure 15 shows the correlation between d_i and γ_i while Figures 16 and 17 show their individual distributions. Each of these sets of figures is made for an isotropic muon distribution.

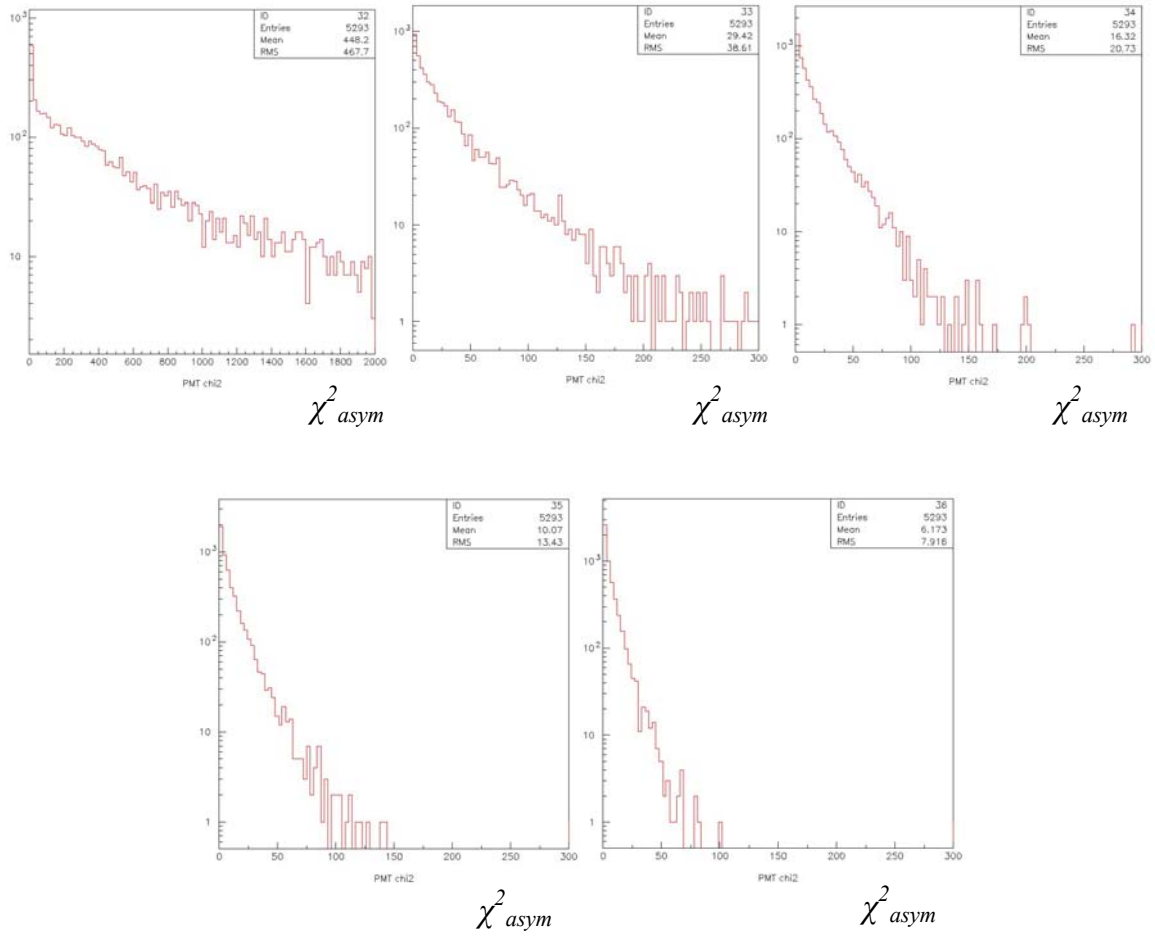

Figure 14. Distribution of χ^2_{asym} (isotropic case) in each of the first five FADC bins (from top left to bottom right).

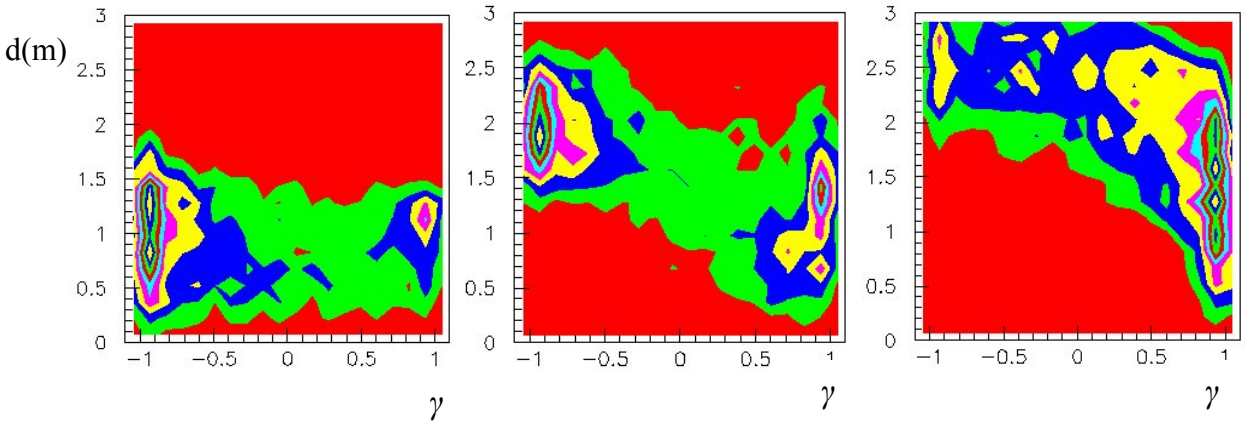

Figure 15. Distributions of d_i and γ_i (isotropic case) showed separately for the PMT having the largest first bin charge (left), that having the second larger (middle) and that having the smallest (right).

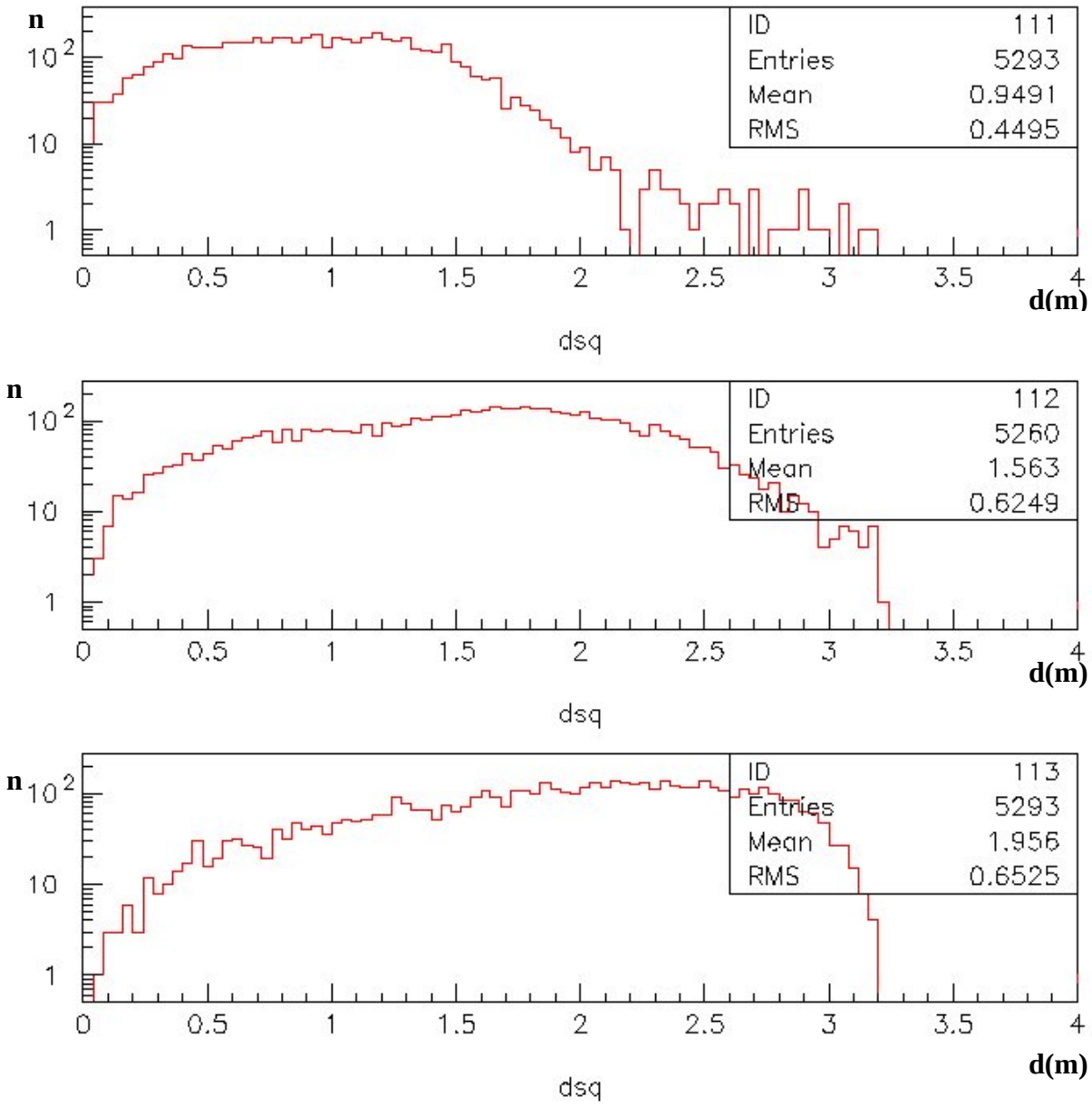

Figure 16. Distributions of d_i (isotropic case) shown separately for the PMT are having the largest first bin charge (top), that is having the second larger (middle) and that having the smallest (bottom).

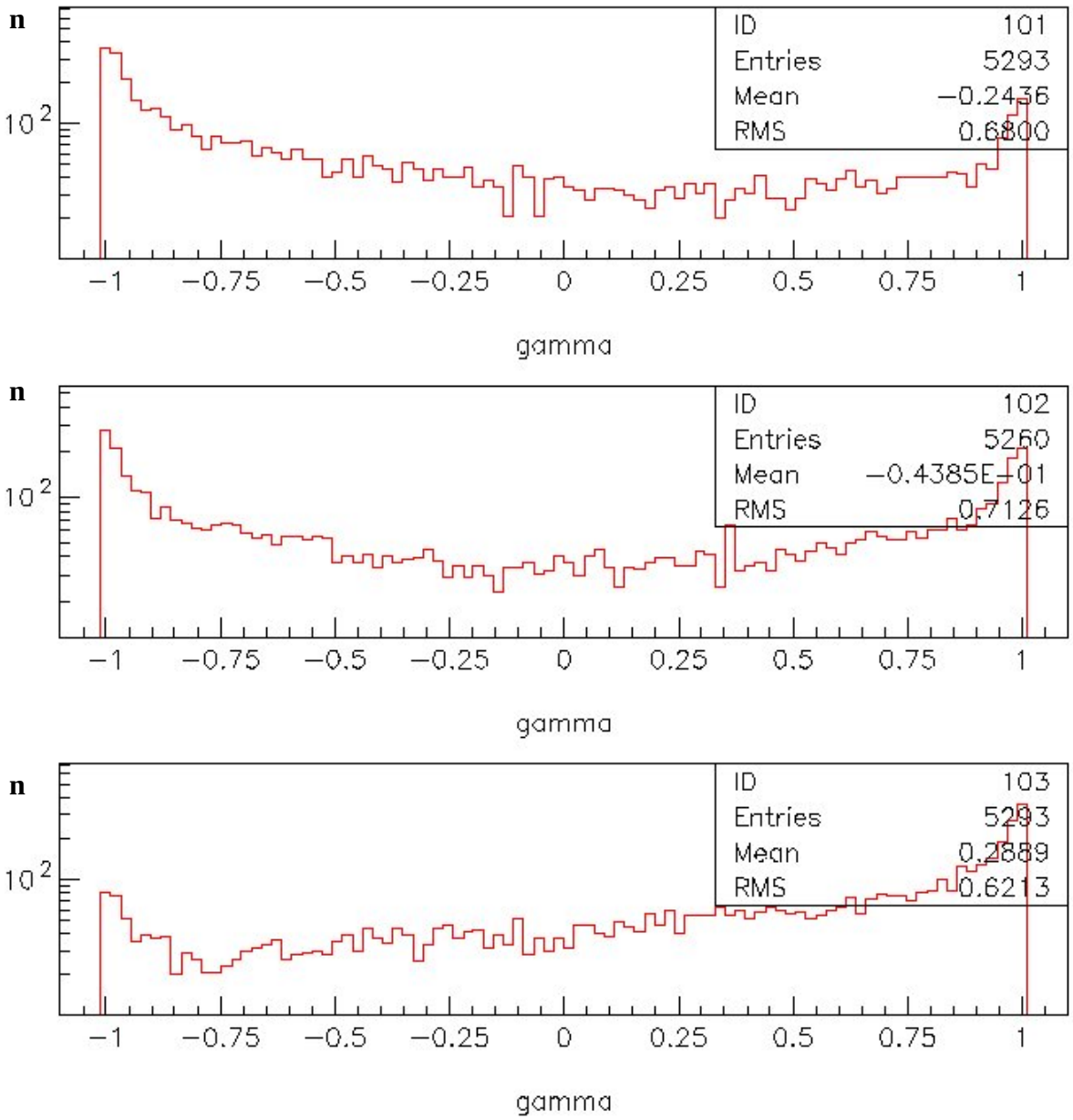

Figure 17: Distributions of γ_i (isotropic case) showed separately for the PMT having the largest first bin charge (top) that having the second larger (middle) and that having the smallest (bottom).

3.2 Using the asymmetry information in real data

Figure 15 has shown very clearly that the asymmetry is associated with both the azimuth of the incident muon and the location of its impact point. In real data the azimuth of the shower particles entering the tank can be approximated by that of the shower (evaluated, as explained earlier, from the different times of arrival measured in the tanks hit). However no information is available on the location of the impact point. If a correlation between asymmetry and azimuth is clearly present in the real data [17], it is unfortunately smeared by the unknown distribution of impact points: the asymmetry cannot be used simply on an event by event basis to contribute to the azimuth measurement.

However, another more interesting use of the asymmetry is possible in the analysis of the FADC traces: an asymmetry can be used, in principle, to tag the start of a new signal. In cases where many signals overlap on a same trace, this is very valuable information. Indeed, the decay time of any individual signal is expected to be always the same, it only depends on the optical properties of the tank, and knowing in which bin a new signal starts enables one to define its contribution to the trace as a function of a single parameter, its amplitude. A question then arises: how reliable is the asymmetry information to tag new signals? In particular, to which extent can one trust that each new signal is associated with an important asymmetry? We know already from the χ^2_{asym} distribution shown in Figure 13 that it may happen that the early light shows no asymmetry, corresponding to a low χ^2_{asym} value. How often does it happen? And what is it due to? To answer the first question we compare in Figures 18 and 19 the $cos\theta$ and track length distributions of all events with those of events where the first bin value of χ^2_{asym}, χ^2_{asym1}, does not exceed 30. These events amount to 13.4% of the total. While the $cos\theta$ dependence of the asymmetry is moderate (the ratio between the two populations varies from 3% at horizontal incidence to 8% at vertical incidence with a maximum at 16% near 65^o), its dependence on track length is important: smaller track lengths, namely smaller signals, are less asymmetric. Nearly all cases where χ^2_{asym1} does not exceed 30 have track lengths smaller than 70 cm.

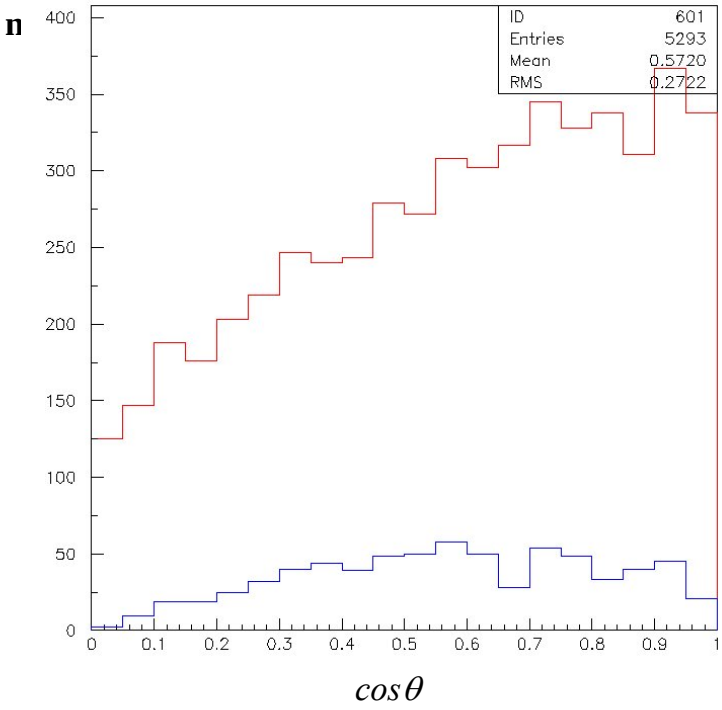

Figure 18. Distribution in $cos\theta$ of events (lower histogram) where χ^2_{asym1} does not exceed 30 compared to all events (upper histogram).

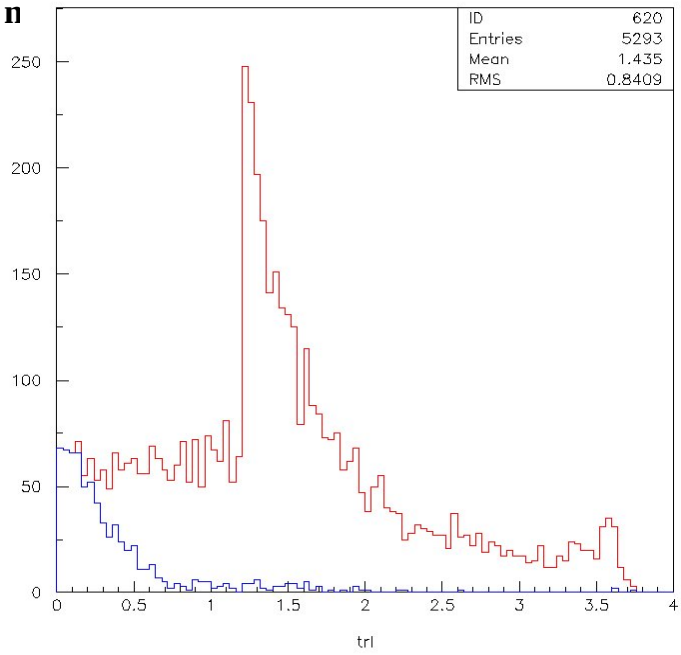

Figures 19: Track length distribution of events where χ^2_{asym1} does not exceed 30 (lower histogram) compared to all events (upper histogram).

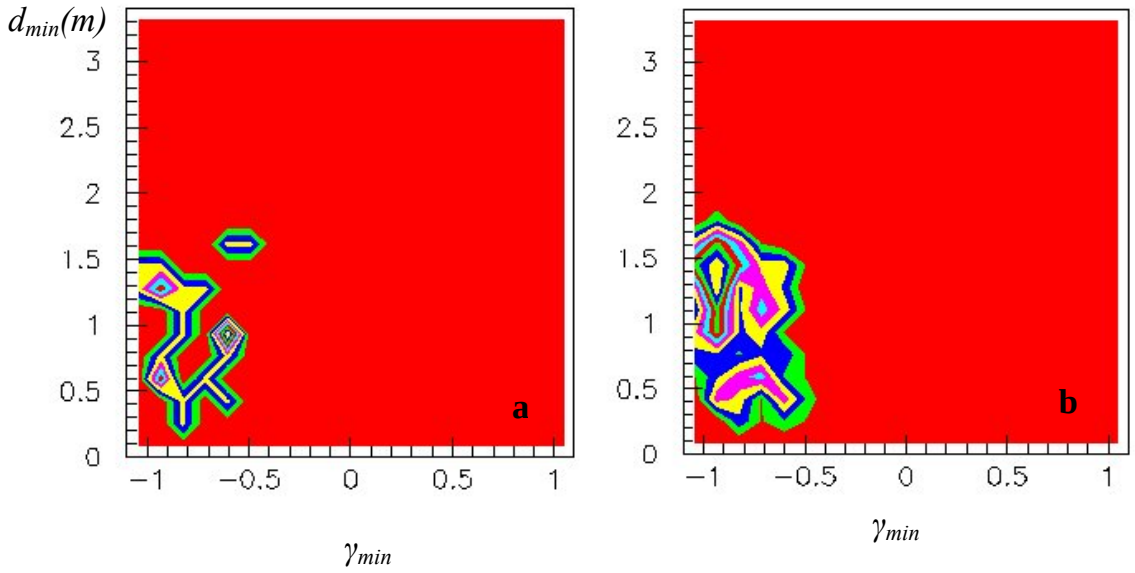

Figure 20: Distribution in the (d_{min},γ_{min}) plane of events having χ^2_{asym1} <30.
a) Events where the minima of d_i and γ_i occur in the same PMT.
b) Events where the minima of d_i and γ_i occur in different PMTs.

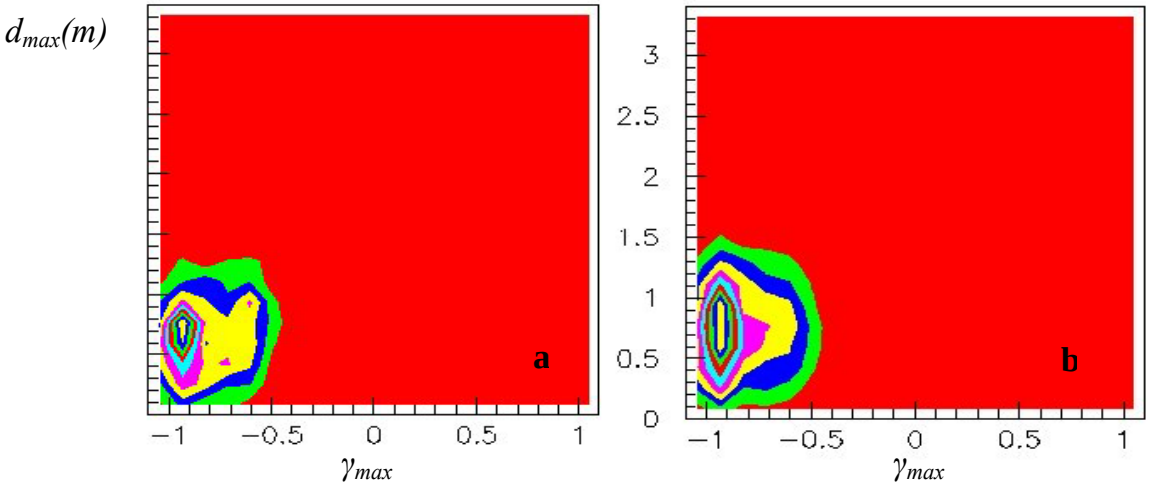

Figure 21: Distribution in the (d_{min},γ_{min}) plane of events having χ^2_{asym1} >30.
a) Events where the minima of d_i and γ_i occur in the same PMT.
b) Events where the minima of d_i and γ_i occur in different PMTs.

We therefore only retain events having both a bad asymmetry (χ^2_{asym1}<30) and not too small a track length (>0.4 m). Such events amount to 3.9% of the total or 4.4% of events having a track length in excess of 0.4 m (the requirement of having a track length in excess of 0.4 m retains 88.4% of all events). For these, as χ^2_{asym1} is small, it

is no longer meaningful to distinguish between PMTs having the largest, middle and smallest signal. It is more meaningful to look for the PMT having the smallest d_i value and that having the smallest γ_i value. One should distinguish between events where the two PMTs differ or are the same. In the first case, the two effects conspire to lower the asymmetry while in the second case they act coherently to increase the asymmetry. Indeed, for events having χ^2_{asym1} smaller than 30, the same PMT has the smallest d value and the smallest γ value in 11% of the cases; while, for events having χ^2_{asym1} in excess of 30, the same PMT has the smallest d value and the smallest γ value in 21% of the cases, nearly twice as often. This is illustrated in Figures 20 and 21(above). Calling d_{min} the minimum values of d_i and γ_{min} the minimum value of γ_i, Figure 20 shows the distribution of the events in the (d_{min}, γ_{min}) plane for events where the minima of d_i and γ_i occur in the same (Figure 20 a) or in different (Figure 20 b) PMTs. Figures 21 a and b show the same distributions for events having χ^2_{asym1} in excess of 30 (but still a track length in excess of 0.4 m).

SUMMARY AND PERSPECTIVES

The present study has provided a simple description of the main optical properties of the Cherenkov counters used in the Pierre Auger Observatory for the detection of ultra high energy cosmic rays.

The main features of the signals produced by charged particles traversing the tank have been neatly reproduced, in particular the fast rise followed by an exponential decay. The decay time is characteristic of each tank and is fully governed by the attenuation length in water and the absorption in the tank walls. The values used here (100 m and 5% respectively) give reasonable average results and it would be simple to adjust them globally for each tank independently. The averaging over wave lengths was sufficient for the purpose of the present study. It might be that a study of the wave length dependence, which is different for the attenuation in water and the diffusion on the walls, would allow for an independent tuning of these two quantities. This, however, would not be as simple as what has been done here and, if at all possible, is clearly beyond the scope of the present work.

The evidence for an asymmetry between the early parts of the signals recorded in the three PMTs of a same tank is a particularly interesting result. Such an asymmetry had indeed been found in the real data and the correlation with the shower azimuth had already been established. The present simulation provides a convenient tool to understand the effect when comparing its prediction to real data. Particularly useful is the evaluation of the probability for a new signal to show a significant asymmetry. The present study has shown that this probability was very high. Once short track lengths (meaning low signals) are ignored (at the level of 12% for the choice of cut that was used here) most cases (over 95% with the present choice of cuts) display a high asymmetry. A precise evaluation of these numbers needs to be done on real data, redefining χ^2_{asym1} in a way that accounts for measurement uncertainties. The asymmetry may then be used, with an efficiency that can be precisely quantified, to help the identification of overlapping signals in the FADC traces. This is an invaluable asset as the disentangling of FADC traces into separate signals is an essential step in the detailed analysis of PAO data. It is the subject of the PhD thesis of a member of VATLY [18] and the Monte Carlo code that has been developed here, after the addition of some minor refinements, will be a very useful tool for this purpose.

REFERENCES

[1] M.S. Longair, *High Energy Astrophysics,* Cambridge University Press, 1992.

[2] T.K. Gaisser *et al*., *Cosmic Rays and Particle Physics,* Cambridge University Press, 1990.

[3] L. Anchordoqui *et al*., *High Energy Physics in the Atmosphere: Phenomenology of Cosmic Ray Air Showers,* NUB-3245/Th-04, La Plata-Th-04-03, hep-ph/0407020.

[4] H, Muraishi *et al*., Prog.Theor.Phys. 113 (2005) 721-731.

[5] K. Greisen, Phys. Rev. Lett. 16, 748 (1966).

[6] G. T. Zatsepin and V. A. Kuzmin, JETP Lett. 4, 78 (1966) [Pisma Zh. Eksp. Teor. Fiz. 4, 114 (1966)].

[7] K. Sakurai, *Physics of Solar Cosmic Rays,* University of Tokyo Press, 1974.

[8] G. Rowell, Journal of Phys.: Conference Series 47 (2006) 21–30.

[9] D. Harari *et al*., *Correlation of cosmic rays with astronomical objects in the Pierre Auger Observatory data*, Auger Note GAP-2006-046 (2006).

[10] J.D.Hague *et al*., *Search for Correlations between nearby AGNs and Auger data*, Auger Note GAP-2006-047 (2006).

[11] The Auger Collaboration, Nucl. Instr. Meth. A 523, 50 (2004).

[12] P.N. Diep, Master thesis,

http://www.vaec.gov.vn/inst/English/About/VATLY/Vatly.htm

P.N.Diep et al., Comm. Phys., Volume 16, Number 3, 129-143.

[13] S. Eidelman et al., Phys. Lett. B592 (2004) 1,W. R. Leo, Techniques for Nuclear and Particle Physics Experiments, Springer Verlag, 1994.

W.R. Leo, Techniques for nuclear and particle physics experiments, Springer-Verlag, 1994

[14] Pierre Auger Observatory, "The Pierre Auger Project Technical Design Report", September 2001.

J. Abraham, et al., Pierre Auger Collaboration, Nucl. Inst. meth. A523 (2005) 50.

[15] PTT Nhung, “Performance studies of water Cherenkov counters ”, master thesis, Hanoi, 2006. http://www.vaec.gov.vn/inst/English/About/VATLY/Vatly.htm

[16] *P. Billoir***,** “The muon hump in real shower data from the Surface Detector”, Internal note of the Auger Collaboration, GAP-2005-004.

[17] P.T. Nhung, VATLY Internal note 19 and references therein.

[18] P.T. Nhung, Ph D thesis, in progress.